Fundamental bounds on the operation of Fano nonlinear isolators

Dimitrios L. Sounas[1] and Andrea Alù[1,2,3,4,*]

[1]*Department of Electrical and Computer Engineering, The University of Texas at Austin, Austin, Texas 78712, USA*
[2]*Photonics Initiative, Advanced Science Research Center, City University of New York, New York 10031, USA*
[3]*Physics Program, Graduate Center, City University of New York, New York 10016, USA*
[4]*Department of Electrical Engineering, City College of The City University of New York, New York 10031, USA*

Nonlinear isolators have attracted significant attention for their ability to break reciprocity and provide isolation without the need of an external bias. A popular approach for the design of such devices is based on Fano resonators, which, due to their sharp frequency response, can lead to very large isolation for moderate input intensities. Here, we show that, independent of their specific implementation, these devices are subject to fundamental bounds on the transmission coefficient in the forward direction versus their quality factor, input power, and nonreciprocal intensity range. Our analysis quantifies a general tradeoff between forward transmission and these metrics, stemming directly from time-reversal symmetry, and that unitary transmission is only possible for vanishing nonreciprocity. Our results also shed light on the operation of resonant nonlinear isolators, reveal their fundamental limitations, and provide indications on how it is possible to design nonlinear isolators with optimal performance.

I. INTRODUCTION

Nonreciprocal devices, such as isolators and circulators, are crucial components in optics, of great interest for source protection, and to separate signals propagating in opposite directions [1,2]. Reciprocity can be broken by either biasing a linear structure with a quantity that is odd-symmetric under time reversal or relying on nonlinear effects [3]. The most common approach consists in applying an external static magnetic bias, but other magnetless approaches based on biasing with electric current or linear or angular momentum have recently gained attention for their potential to realize integrated low-noise isolators and circulators [4–17]. Nonlinearities can also enable magnetless nonreciprocal components, with the advantage of not requiring an external bias, thus realizing all-passive nonreciprocity [18–38]. In this context, nonlinear isolators exhibit a large transmission contrast when excited from opposite sides with signals of equal intensities. These devices are self-biased by the signal itself traveling through the device, and therefore they can provide isolation only when excited separately from different ports [37], in contrast to linear isolators that work under any excitation condition, even with signals incoming simultaneously from both ports. Yet, these nonlinear devices can be very useful in situations involving pulsed signals. A relevant scenario of interest is the case of a nonlinear isolator connected at the output of a pulsed source. If the pulse duration is short enough, the overlap between the incident signal from the source and the reflected signal at the output of the isolator can be avoided, allowing the nonlinear isolator to transmit the incident signal and block the reflected one. The most common way to achieve nonlinear isolation is through the optical Kerr effect, according to which the permittivity of a material depends on the local intensity of

the electric field as $\varepsilon = \varepsilon_{\mathrm{lin}} + \chi^{(3)}|\mathbf{E}|^2$, where $\varepsilon_{\mathrm{lin}}$ is the linear permittivity, $\chi^{(3)}$ is the third-order nonlinear susceptibility, and $\mathbf{E}$ is the local electric-field intensity. If a Kerr resonator is designed to support different field distributions when excited from opposite directions, the nonlinear permittivity distribution ensures an asymmetry in response and, by appropriate design, full isolation can be achieved.

A common approach for the design of Kerr nonlinear isolators is based on two-port nonlinear resonators with asymmetric coupling coefficients from opposite ports. Fano resonators are ideal in this context, as they offer a sharp frequency response, with transmission varying from zero to a peak over a narrow frequency band around the resonance frequency, which enables the design of nonlinear isolators with very large isolation for moderate input intensity [31–36]. In this context, isolation is defined as the ratio of transmission in opposite directions for the same input intensity; infinite isolation corresponds to zero transmission from one direction and nonzero transmission from the opposite one. Indeed, the vast majority of nonlinear isolators presented to date in the literature are based on devices that fall in the broad category of Fano resonators.

In the following, we show that this large class of nonlinear isolators is subject to bounds stemming directly from time-reversal symmetry and passivity—which fundamentally limit their forward transmission T_{fw} versus their nonreciprocal intensity range (NRIR), defined as the ratio of intensities from opposite directions for which transmission experiences a fast transition from low/high to high/low values—the Q factor, and the input intensity P_{in}. A large NRIR implies a large range of intensities offering strong isolation, while a unitary NRIR corresponds to a structure with the same response from opposite sides, and therefore no isolation at all. In the following, we first rigorously prove that in resonant nonlinear isolators reversing the propagation direction results in a direct scaling of the intensity that leads to a given transmission value, by a factor that is exactly equal to the degree of asymmetry

*aalu@gc.cuny.edu
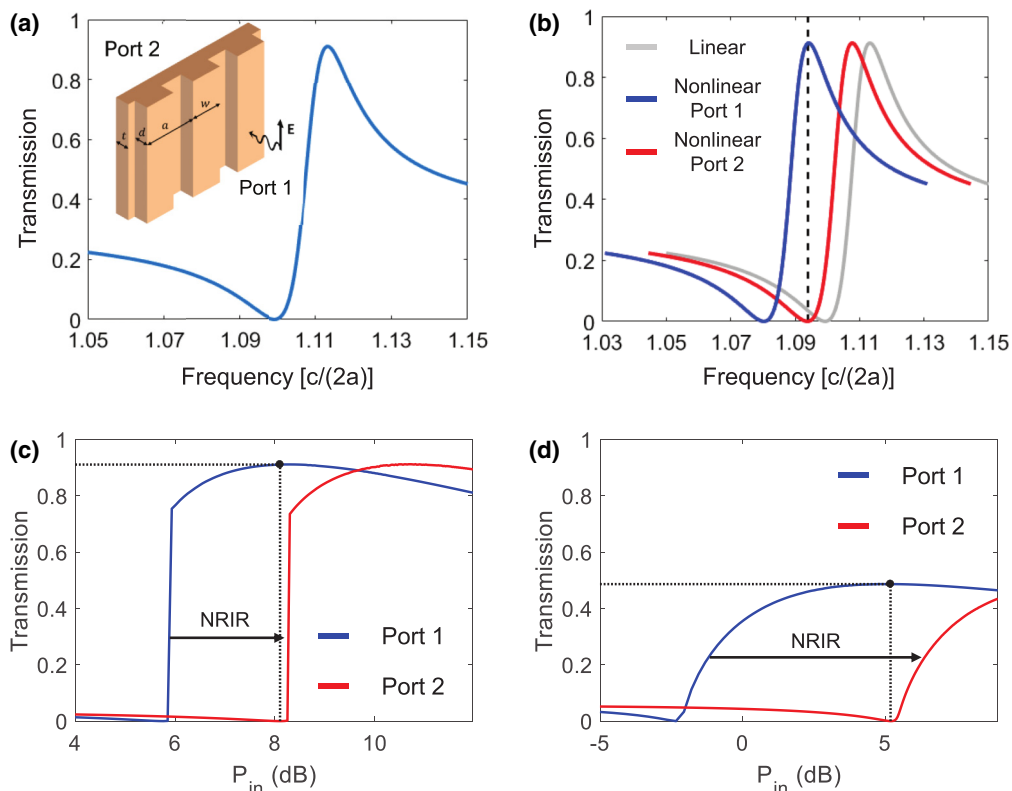
FIG. 1. Nonlinear Fano isolator based on a substrate-backed dielectric grating. (a) Linear response and schematic of the structure for $d = 0.1a$, $w = 0.8a$, $t = 0.03a$, and $\varepsilon_{\text{lin}} = 12$. (b) Desired nonlinear response, for which a transmission maximum from port 1 is aligned in terms of input intensity with a zero from port 2. The vertical dashed line indicates the excitation frequency. (c) Actual nonlinear response for the same parameters as in panel (a), excitation frequency $f = 1.094c/(2a)$, and third-order nonlinear susceptibility $\chi^{(3)} = 2.8 \times 10^{-18} \text{ m}^2/\text{V}^2$. (d) Similar to panel (c) but for $t = 0.08a$ and $f = 0.9575c/(2a)$. The numerical results were derived through full-wave simulation with COMSOL MULTIPHYSICS.

with which the two ports are coupled to the resonator in the linear regime, showing that NRIR is identically equal to the linear asymmetry factor. Combining this property with a general bound between transmission and the asymmetry factor that can be derived from time-reversal symmetry, we show that, independent of the specific design strategy, T_{fw} necessarily decreases as NRIR increases, and that $T_{\text{fw}} = 1$ only for vanishing nonreciprocity. In other words, it is impossible to realize Fano nonlinear isolators with unitary transmission. We also derive tight bounds on T_{fw} as a function of Q and P_{in} for the case of infinite isolation (the case when backward transmission is zero), showing that an increase in T_{fw} requires increasing Q factor and/or input intensity. Our analysis also provides insights on the general operation of nonlinear isolators, and a quantitative tool to design optimal devices with the largest possible forward transmission for given Q factor, bandwidth, input power, and nonreciprocity intensity range.

II. TRADEOFF BETWEEN TRANSMISSION AND ISOLATION INTENSITY RANGE

In order to understand the nature of the limitations outlined above, we start from a particular example of a Fano nonlinear isolator, based on a substrate-backed dielectric grating, as in the inset of Fig. 1(a). Such a design is suitable for isolation of

waves propagating in free space. The structure has $\varepsilon_{\text{lin}} = 12$, $\chi^{(3)} = 2.8 \times 10^{-18} \text{ m}^2/\text{V}^2$, realistically modeling Si [39], and it is excited from the normal direction with a wave polarized parallel to the grating. Figure 1(a) shows the linear response of the structure, with a Fano resonant signature stemming from the superposition of a high-Q resonance in the dielectric rods and a low-Q background reflection at the air-dielectric interfaces [40], with transmission rapidly changing from zero to a peak as the input frequency varies. The grating depth d, width w, and periodicity a control the resonance frequency, while the substrate thickness t controls the asymmetry from opposite sides, necessary to realize isolation in the nonlinear regime. Increasing the input intensity results in an increase of permittivity due to Kerr nonlinearity, which in turn shifts downwards the resonance frequency. Since the resonator is asymmetric, this shift is different for excitation from opposite sides, enabling isolation. The isolation becomes infinite when the input intensity is selected so that the resonant dip for excitation from one side (left-hand side in Fig. 1) aligns with the operation frequency. Through appropriate design of the structure asymmetry, we can also make sure that, for excitation from the other side (right-hand side in Fig. 1), the resonance peak arises for the same intensity at the same excitation frequency, enabling an isolator with zero and maximum transmission for opposite excitations. Figure 1(b) illustrates this

mechanism, comparing the linear response (gray) with the nonlinear responses for excitation with same input intensity from opposite sides. Ideally, we would like to achieve unitary transmission in the forward direction (T_{fw}) and large isolation over a broad intensity range.

Consider now the calculated response of this nonlinear grating, presented in Fig. 1(c). The figure shows transmission versus input intensity for the desired excitation frequency. The substrate thickness t was selected to a finite value to provide nonzero asymmetry, while the rest of the design parameters were chosen to maximize T_{fw} when transmission in the backward direction is zero. For both directions, as we increase the input intensity the transmission experiences a rapid transition from low to high values at a particular input intensity (from now on, we will call this intensity the critical intensity), corresponding to the Fano feature crossing the excitation frequency. Due to the resonator asymmetry, the transition intensity is different for opposite excitations, leading to large isolation for input intensities between the critical intensities for opposite directions. We define the ratio of critical intensities from opposite directions as the nonreciprocal intensity range, which, as mentioned in the introduction, quantifies the range of intensities over which large transmission contrast from opposite directions can be achieved. One natural way to increase NRIR is to increase the asymmetry parameter t. In Fig. 1(d), we show the transmission for a substrate with larger thickness, with the other design parameters optimized again to maximize T_{fw} at the intensity of infinite isolation. Although a larger t indeed increases NRIR, this increase results in an unwanted decrease in forward transmission, degrading the overall performance of the device.

This tradeoff between forward transmission and NRIR, evident in the example of Fig. 1, is not specific to this design, but it is very general, and it can be understood using coupled-mode theory (CMT). In the context of CMT, a two-port lossless Fano resonator is described as [34]

$$\frac{da}{dt} = (i\omega_0 - \gamma)a + k_1 s_1^+ + k_2 s_2^+,$$
$$s_1^- = r_B s_1^+ + i t_B s_2^+ + k_1 a, \qquad (1)$$
$$s_2^- = r_B s_2^+ + i t_B s_1^+ + k_2 a,$$

where a is the resonance amplitude, ω_0 is the resonance frequency, γ is the decay rate, k_i is the coupling coefficient between the resonator and the ith port, s_i^+ is the signal entering the resonator from the ith port, s_i^- is the signal leaving the resonator from the ith port, r_B is the background reflection coefficient, and t_B is the background transmission coefficient. r_B, t_B refer to the response of the system far from the Fano resonance [41]. Notice that this model encompasses also Lorentzian resonators, as a particular class of Fano resonators.

The decay rate can be decomposed as $\gamma = \gamma_1 + \gamma_2$, where γ_1, γ_2 are the decay rates due to radiation to the ports. Equation (1) needs to be supplemented with the conditions $2\gamma_i = |k_i|^2$, $|r_B|^2 + |t_B|^2 = 1$ and

$$\begin{pmatrix} r_B & i t_B \\ i t_B & r_B \end{pmatrix} \begin{pmatrix} k_1^* \\ k_2^* \end{pmatrix} = -\begin{pmatrix} k_1 \\ k_2 \end{pmatrix}, \qquad (2)$$

derived from power conservation and time-reversal symmetry. From Eqs. (1) and (2), it is straightforward to find that the

transmission coefficient through the system is given by

$$T = T_B \frac{(x \mp x_0)^2}{x^2 + 1}, \qquad (3)$$

where $T_B = |t_B|^2$, $x = (\omega_0 - \omega)/\gamma$ is the detuning factor of the resonator, ω is the driving frequency, and $x_0 = \sqrt{4\gamma_1\gamma_2/[T_{bg}(\gamma_1 + \gamma_2)^2] - 1}$ is a characteristic parameter of the resonator that provides the detuning from the resonance frequency at which transmission is zero. The minus sign in Eq. (3) corresponds to the case where the transmission zero is at lower frequencies than the resonance frequency, as in Fig. 1, which also implies that the transmission zero is at a lower frequency than the transmission maximum. The plus sign is the dual case of a resonator with the transmission zero at a higher frequency than the resonance frequency.

If we define $\kappa = |k_1|^2/|k_2|^2 = \gamma_1/\gamma_2$ as the asymmetry factor from different ports (κ can also be defined as the ratio of field intensities for excitation from different ports; assuming operation close to a single resonance, this ratio is the same at any point in the resonator, as we are assuming a single mode), Eq. (3) can be rewritten as

$$T = \frac{4\kappa}{(\kappa + 1)^2} \frac{(x \mp x_0)^2}{(x^2 + 1)(x_0^2 + 1)}. \qquad (4)$$

If the resonator is symmetric, $\kappa = 1$ and $T = \frac{(x \mp x_0)^2}{(x^2+1)(x_0^2+1)}$, which shows that the effect of asymmetry is to scale transmission by the factor $\frac{4\kappa}{(\kappa+1)^2}$, while leaving its line shape unaffected. Considering that for a symmetric Fano resonator maximum transmission is unitary, we see that asymmetry imposes the following bound on the transmission of Fano resonators:

$$T \leqslant \frac{4\kappa}{(\kappa + 1)^2}. \qquad (5)$$

In [42,43], it was shown that this equation actually applies to any lossless linear structure, regardless of whether it is a Fano resonator or not, and it is a direct consequence of time-reversal symmetry. For Fano resonators, Eq. (5) also applies to the lossy case, which can be intuitively explained by the fact that adding loss reduces maximum transmission compared to the lossless case. A rigorous proof of this fact can be developed as in the lossless case after adding the intrinsic decay rate γ_{loss} of the resonator to γ.

Consider now a quadratic nonlinearity $\varepsilon = \varepsilon_{lin} + \chi^{(3)}|\mathbf{E}|^2$ in the Fano resonator. The nonlinearity results in a shift of the resonance frequency of the resonator as

$$\omega_0 = \omega_{0,lin}\left(1 - \frac{|a|^2}{|a_0|^2}\right), \qquad (6)$$

where $\omega_{0,lin}$ is the resonance frequency in the linear (low-intensity) regime and $|a_0|^2$ is a characteristic quantity of the resonator with units of energy [41]. In principle, the nonlinearity may also affect the decay rate γ and the coupling coefficients k_i between the resonator and the ports, however these effects are usually neglected for perturbations involving only the real part of the permittivity, since γ and k_i are primarily determined by the mode profile which, compared to the resonance frequency, is weakly affected by the nonlinearity [41,44]. This allows applying Eq. (3) to the nonlinear case, if

we replace ω_0 with the expression in Eq. (6), with the rest of the parameters (γ, T_{bg}, κ) being calculated in the linear regime. Then, Eqs. (4) and (5) also hold in the nonlinear case, with the parameter κ, determining the bound, still being the asymmetry factor in the *linear* regime. Consider now that the structure is excited from the ith port with a monochromatic signal s_i^+ at frequency ω. Then, the resonance amplitude is given by

$$a = \frac{k_i}{i(\omega - \omega_0) + \gamma} s_i^+, \tag{7}$$

where the only quantity that depends on the input intensity is ω_0, while γ and k_i are the same as in the linear regime. Inserting Eq. (7) into Eq. (6) yields

$$\left(1 - \frac{\omega_0}{\omega_{0,\mathrm{lin}}}\right)\left[(\omega - \omega_0)^2 + \gamma^2\right] = \frac{|k_i|^2 P_i^{\mathrm{in}}}{|a_0|^2}, \tag{8}$$

where $P_i^{\mathrm{in}} = |s_i^+|^2$. From Eq. (8), we can derive a very important property for the response of Fano nonlinear isolators. In particular, the resonance frequency, and consequently the overall response of the resonator, for excitation from port 2 has exactly the same dependence versus intensity as for excitation from port 1, if the input intensity is scaled by the factor $\kappa = |k_1|^2/|k_2|^2$, again depending exclusively on the response of the isolator in the linear regime. In other words, the blue and red curves in Figs. 1(c) and 1(d), and for any arbitrary Fano nonlinear isolator, can be derived from each other by simply horizontally scaling by a factor κ, which we stress again is the *linear* asymmetry parameter. This property shows that NRIR, defined earlier as the ratio of transition intensities from opposite directions, is also the ratio of input intensities from opposite directions that lead to the same transmission coefficient for any value of the transmission coefficient. Furthermore, NRIR is equal to κ or κ^{-1} depending on whether $\kappa > 1$ or $\kappa < 1$, respectively. In a decibel scale, NRIR is equal to the difference of input powers in decibels that yield the same transmission from opposite directions. A unitary NRIR (zero in dB scale) corresponds to a system with identical response from opposite sides and therefore no isolation. On the other hand, a large NRIR corresponds to a system which exhibits large isolation over a large range of input intensities, as in Figs. 1(c) and 1(d).

The fact that Eq. (5) is valid in the nonlinear case and that the linear κ involved in these equations gives NRIR results in a fundamental bound between nonlinear transmission and NRIR. In particular, plugging κ from NRIR $= \max\{\kappa, \kappa^{-1}\}$ into Eq. (5) yields

$$T \leqslant \frac{4\mathrm{NRIR}}{(\mathrm{NRIR} + 1)^2}. \tag{9}$$

This equation shows that increasing T is only possible by reducing NRIR, consistent with the examples in Figs. 1(c) and 1(d). The extreme case of unitary transmission is possible only
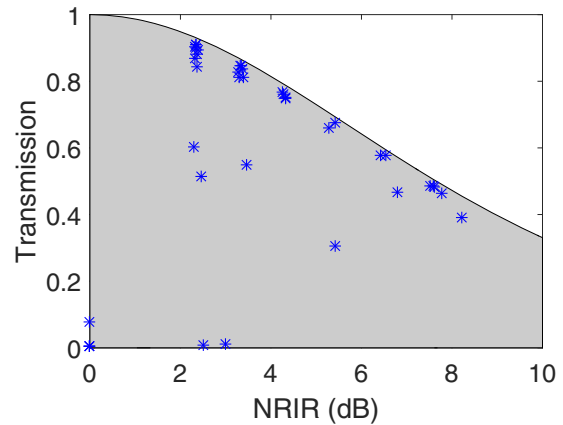
FIG. 2. Transmission in the forward direction vs nonreciprocal intensity range for various nonlinear isolator designs in Fig. 1. The shaded region corresponds to the bound in Eq. (9).

for $\kappa = 1$, which corresponds to NRIR $= 1$ (0 dB), meaning that it is impossible to realize a Fano-based nonlinear isolator with unitary transmission. In order to numerically validate this result, Fig. 2 shows T_{fw} at the intensity of infinite isolation versus NRIR calculated for various design parameters for the nonlinear metasurface in Fig. 1, fully validating Eq. (9), and confirming that our derived bound is tight. We would like to highlight that Eq. (9) is a consequence of the special nonlinear dynamics of Fano resonators, namely, the applicability of Eq. (5) in the nonlinear case and the close relation between NRIR and the linear κ. Since any system with a single resonator can be accurately mapped to a Fano response (for example, a Lorentzian resonator is a Fano resonator with zero or unitary background transmission), it follows that Eq. (9) is also valid for any isolator based on a single resonator. In turn, this fact indicates that Eq. (9) may be possibly broken in more complex systems consisting of multiple resonators [45] or other systems that do not involve resonators at all [38], although such systems will still be subject to the dynamic reciprocity limitations described in Ref. [37]. It is important to note that Eq. (9) is also valid for lossy resonators, since, as we explained before, Eq. (5) still holds in the case of loss, and Eq. (8) is unaffected by the presence of absorption, if γ is the total decay rate of the resonator that includes intrinsic loss. The same is true even for the case of two-photon absorption, which becomes important at high input intensities. Two-photon absorption results in an intrinsic loss rate that increases as the input intensity increases as

$$\gamma_{\mathrm{loss}} = \gamma_{0,\mathrm{loss}}\left(1 + \frac{|a|^2}{|a_{0,\mathrm{TBA}}|^2}\right), \tag{10}$$

where $\gamma_{0,\mathrm{loss}}$ is the loss rate in the linear regime and $|a_{0,\mathrm{TBA}}|^2$ is a characteristic quantity of the system with units of energy. Inserting Eq. (10) into Eq. (8) yields

$$\left(1 - \frac{\omega_0}{\omega_{0,\mathrm{lin}}}\right)\left\{(\omega - \omega_0)^2 + \left[\gamma_0 + \gamma_{0,\mathrm{loss}}\frac{|a_0|^2}{|a_{0,\mathrm{TBA}}|^2}\left(1 - \frac{\omega_0}{\omega_{0,\mathrm{lin}}}\right)\right]^2\right\} = \frac{|k_i|^2 P_i^{\mathrm{in}}}{|a_0|^2}. \tag{11}$$
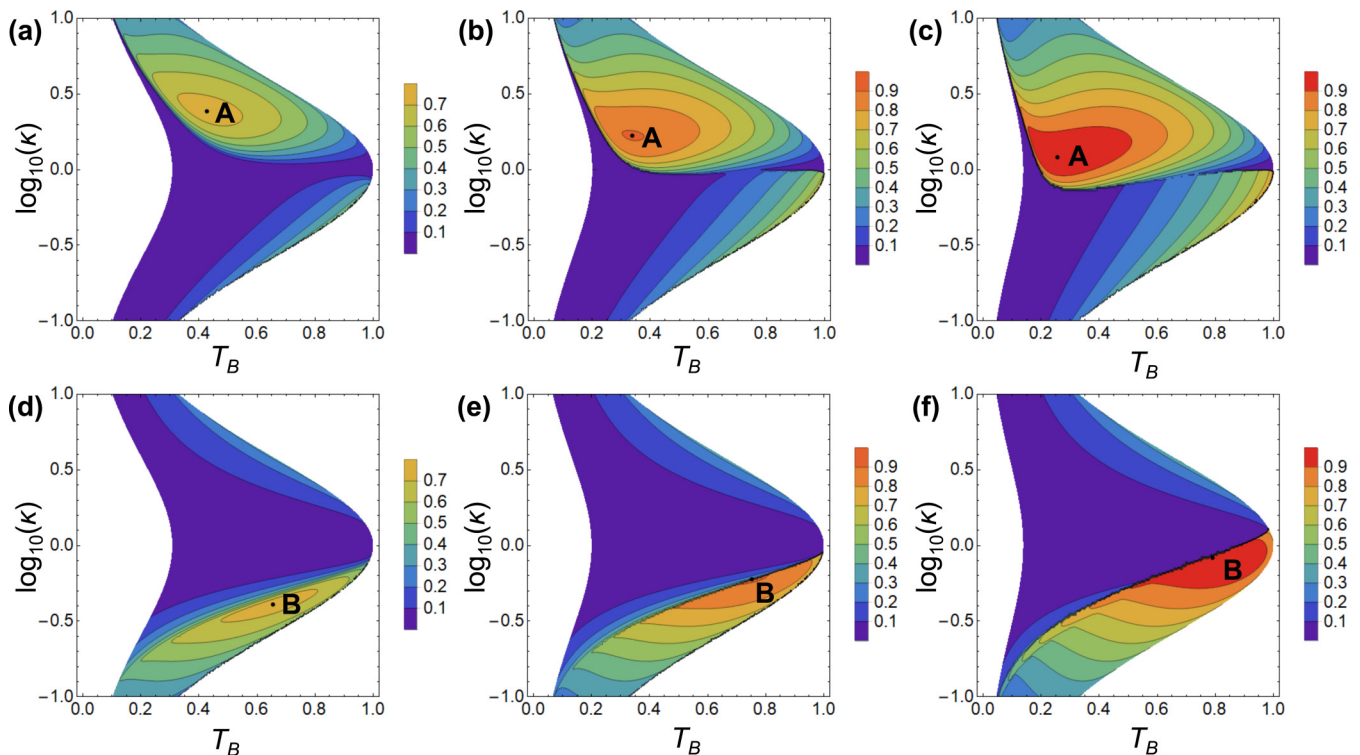
FIG. 3. T_{fw} vs T_B and κ for various values of Q, $\omega_{0,\mathrm{lin}} = 1$, and $\omega = 0.95$. Each point in the plots corresponds to a design with infinite isolation (zero backward transmission). The white regions are forbidden based on Eqs. (5) and (6). (a)–(c) Minus sign in Eq. (3). (d)–(f) Plus sign in Eq. (3). (a), (d) $Q = 15$. (b), (e) $Q = 20$. (c), (f) $Q = 25$.

III. BOUNDS FOR FORWARD TRANSMISSION IN THE CASE OF INFINITE ISOLATION

In the above discussion, we did not make any assumption regarding the transmission in the backward direction, therefore Eq. (9) is valid independent of the isolation level. In the following, we focus on the case in which the device is designed to achieve zero transmission in the backward direction, hence infinite isolation, for a certain input intensity and derive bounds for forward transmission T_{fw} versus the Q factor of the resonator and the input power. The analysis assumes zero loss, since in the presence of loss, transmission of a Fano resonator never goes to zero and as a result it is impossible to obtain infinite isolation. In the lossy case, the results should be interpreted as an upper bound for forward transmission at the intensity of maximum isolation (minimum backward transmission).

From Eq. (4) we see that transmission is zero when $x = \pm x_0$ or $\omega_0 = \omega \pm \gamma x_0$. Assuming a resonator with specified γ, κ, and T_B, we can calculate the input power that leads to zero transmission in the backward direction and therefore

infinite isolation by substituting this ω_0 in Eq. (8) with $i = 2$. Solving Eq. (8) with $i = 1$ and the same input power gives the nonlinearity-shifted resonance frequency in the forward direction for the input power that yields zero transmission in the backward direction. Substituting this resonance frequency into Eq. (3) provides the value of T_{fw}. In Figs. 3(a)–3(c), we plot T_{fw} calculated as outlined above versus T_B (the background power transmission coefficient) and κ for various levels of Q and $\omega = 0.95\omega_{0,\mathrm{lin}}$ and assuming a positive sign in $\omega_0 = \omega \pm \gamma x_0$ [negative sign in Eq. (3)]. Each point in the plots corresponds to a specific nonlinear isolator design that supports zero transmission in the backward direction, i.e., infinite isolation. It has to be noted that, in general, for each combination of κ and T_B, there might be multiple solutions, from which we choose the one with the larger transmission. The white region on the right corresponds to combinations of T_B and κ that are not admitted by $T_B \leqslant 4\kappa/(\kappa + 1)^2$ [Eq. (5) holds for any frequency, therefore also far from resonance where $T \to T_B$], while the one on the left corresponds to cases for which $\omega_0 > \omega_{0,\mathrm{lin}}$, which according to Eq. (6) are not possible. The discontinuities in the plots indicate multistable regions. This figure shows that, for given Q, there is an optimum combination of T_B and κ (point A) that maximize T_{fw}. Since Figs. 3(a)–3(c) have been derived for a positive sign in $\omega_0 = \omega \pm \gamma x_0$, which corresponds to a resonator with the transmission zero at a lower frequency than the transmission maximum, the point of maximum T_{fw} happens for $\kappa > 1$, so that the transmission maximum from port 1 can be aligned with the transmission zero from port 2. On the other hand, selecting the minus sign in $\omega_0 = \omega \pm \gamma x_0$ leads to the contour

plots in Figs. 3(d)–3(f), where the transmission maximum happens for $\kappa < 1$ (point B), since in this case the transmission zero is at a higher frequency than the transmission maximum. Interestingly, even though the operation schemes associated to points A and B are dual of each other, the forward transmission is identical, and it can be found to be equal to (Appendix A)

$$T_{\text{fw}} = \frac{1}{9 + 17x_{\text{lin}}^2 - 12\sqrt{2}x_{\text{lin}}\sqrt{1 + x_{\text{lin}}^2}} \quad \text{for } x_{\text{lin}} \leqslant 2\sqrt{2},$$

$$T_{\text{fw}} = 1 \quad \text{for } x_{\text{lin}} \geqslant 2\sqrt{2}, \tag{12}$$

where $x_{\text{lin}} = 2Q(\omega_{0,\text{lin}} - \omega)/\omega_{0,\text{lin}}$ is the detuning coefficient in the linear regime. The input power required to achieve this transmission is given by (Appendix B)

$$P_{\max} = \frac{|a_0|^2}{3} \frac{\gamma^2}{\omega_{0,\text{lin}}} \left(1 + x_{\text{lin}}^2\right)\left(3\sqrt{2}\sqrt{1 + x_{\text{lin}}^2} - 4x_{\text{lin}}\right), \tag{13}$$

and the corresponding stored energy in the resonator for the direction of maximum coupling is given by (Appendix A)

$$|a|_{\max}^2 = |a_0|^2 \frac{\gamma}{\omega_{0,\text{lin}}} \sqrt{\frac{2 + \sqrt{3}}{3}\left(1 + x_{\text{lin}}^2\right)}. \tag{14}$$

Equation (12) is a powerful and general result, providing, regardless of the specific design and operation of the isolator, a tight upper bound for the forward transmission T_{fw}, and showing that it depends only on its detuning parameter x_{lin} in the linear regime, which is proportional to the Q factor and to the separation between driving frequency and resonance frequency. This bound grows with x_{lin}. In Figs. 3(a)–3(f), we slowly increase x_{lin} by increasing Q, and we observe how indeed T_{fw} at points A and B consistently increases, following Eq. (12). As Q and T_{fw} increase, these two optimal points move closer and closer to the $\kappa = 1$ axis, consistent with the bound between T_{fw} and κ given by Eq. (5). If $x_{\text{lin}} \geqslant 2\sqrt{2}$, interestingly $T_{\text{fw}} = 1$, but this arises at $\kappa = 1$, consistent with the previous discussion. At this point, the system corresponds to a bistable nonlinear resonator exhibiting zero and unitary transmission for the same input intensity, but it is absolutely symmetric when excited from different ports, and therefore offers no nonreciprocity. From a physical point of view, a larger Q factor is associated with a sharper Fano response (a smaller separation between its transmission maximum and zero), allowing one to achieve alignment of the transmission maximum and zero in the nonlinear case for a smaller asymmetry factor, which according to Eq. (5) allows achieving larger T_{fw}. Increasing the Q factor beyond the value for which $x_{\text{lin}} = 2\sqrt{2}$ offers no advantage, since, although T_{fw} can be unitary, $\kappa = 1$, in agreement with Eq. (5), leading to a structure with purely symmetric response from opposite sides and therefore zero NRIR. Equation (12) is numerically validated in Fig. 4 showing the calculated value of T_{fw} for various nonlinear metasurfaces as in Fig. 1 with different values of x_{lin}.

An increase in x_{lin}, leading to larger T_{fw} and narrower NRIR, can be achieved not only with a larger Q factor but also with a larger detuning $\omega_{0,\text{lin}} - \omega$. This second alternative may appear more attractive, due to limitations that usually exist in realizing large Q factors. Nevertheless, it is possible to show
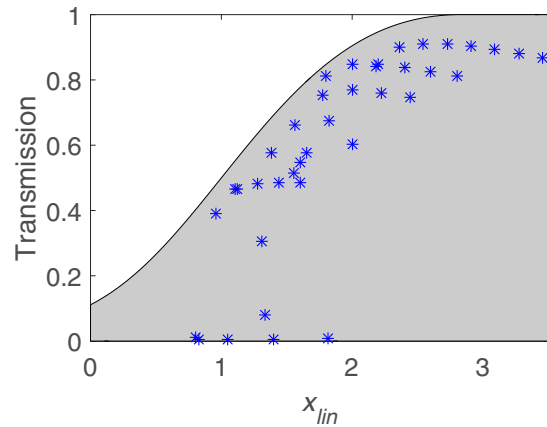
FIG. 4. Transmission in the forward direction vs the detuning factor in the linear regime for various designs of the nonlinear isolator in Fig. 2. The shaded region corresponds to the bound in Eq. (12).

from Eq. (13) that for $x_{\text{lin}} > 0.5$ an increase in x_{lin} through an increase in $\omega_{0,\text{lin}} - \omega$, while γ is kept constant, comes at the price of a larger required input power to reach maximum isolation (Appendix B). This is consistent with the fact that a larger $\omega_{0,\text{lin}} - \omega$ means operation far from linear resonance, requiring a larger input power in order to bring the resonance frequency close to the operation frequency, as it is necessary in order to obtain zero transmission in the backward direction. On the other hand, increasing x_{lin} by increasing the Q factor leads to a reduction of the input power required to achieve maximum isolation (Appendix B). In essence, whatever the specific design we consider, our theory shows that Fano nonlinear isolators are characterized by a fundamental tradeoff between T_{fw} and Q or P_{in}, quantitatively described by Eqs. (12) and (13), which is reflected in a reduction of nonreciprocal intensity range as we increase T_{fw}. Furthermore, it is worth noting that increasing x_{lin} through increasing $\omega_{0,\text{lin}} - \omega$ leads to a linearwise increase of the stored energy versus x_{lin}, as can be seen from Eq. (14) with γ constant, making the system susceptible to two-photon absorption. This effect does not occur when x_{lin} is increased through increasing the Q factor, in which case the stored energy slightly decreases as x_{lin} increases, a fact which can be seen by rewriting Eq. (14) in the form

$$|a|_{\max}^2 = |a_0|^2 \frac{\omega_{0,\text{lin}} - \omega}{\omega_{0,\text{lin}}} \sqrt{\frac{2 + \sqrt{3}}{3}\left(1 + \frac{1}{x_{\text{lin}}^2}\right)} \tag{15}$$

and considering that $\omega_{0,\text{lin}} - \omega$ is constant in this case.

The analysis presented above is valid for monochromatic excitation, while, as mentioned in the Introduction, nonlinear isolators are more suitable for pulsed-source scenarios, due to the dynamic reciprocity limitations pointed out in Ref. [37]. In the following, we show the response of optimal isolators corresponding to points A in Figs. 3(a) and 3(c) for excitation with Gaussian pulses with center frequency $\omega = 0.95$, as in Fig. 3, and envelope $p(t) = \exp(-t^2/\tau^2)$ with $\tau = 1500T$, where $T = 2\pi/\omega$. These pulses are similar to ones used in Ref. [34] to experimentally test the dynamic response of Fano nonlinear isolators at telecom wavelengths. Results are presented for three peak intensities, one corresponding to
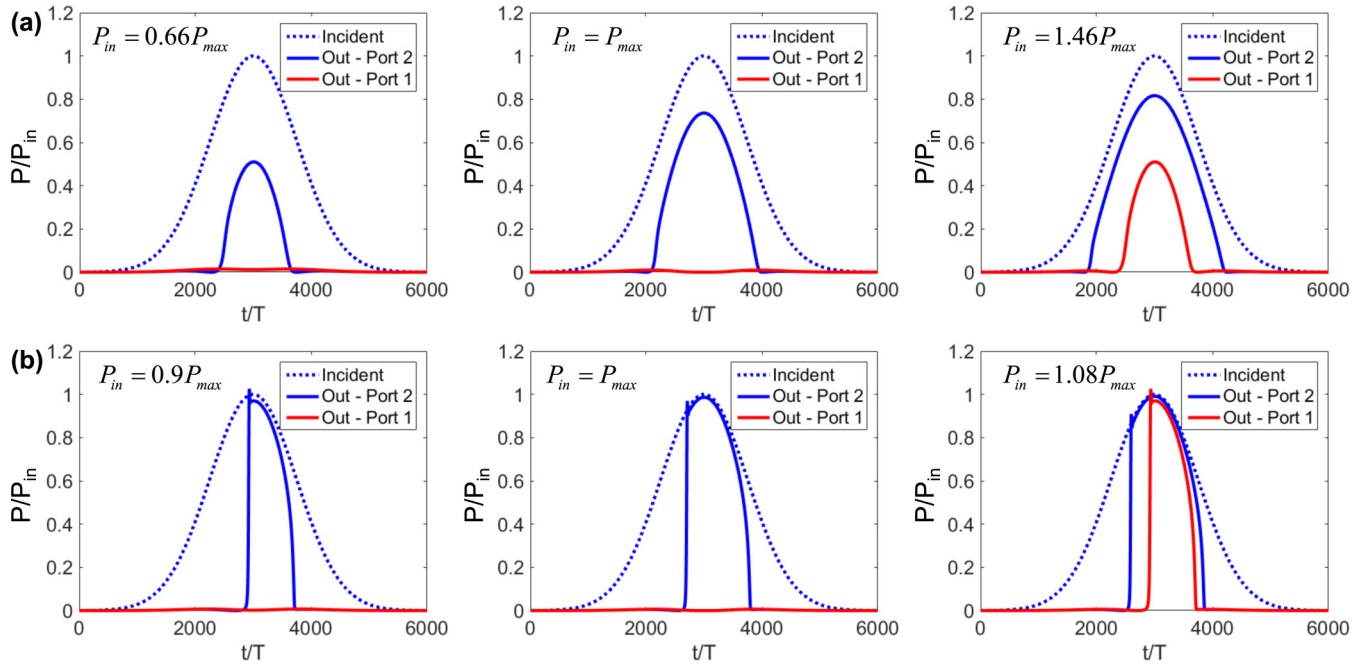
FIG. 5. Time-domain response of a nonlinear isolator for excitation from different ports with a Gaussian pulse. (a) Isolator with the parameters at point A in Fig. 3(a). (b) Isolator with the parameters at point A in Fig. 3(c). P_{in} is the power at the peak of the pulse. P_{max} is the input power of maximum T_{fw} given by Eq. (13).

maximum transmission as calculated from Eq. (13) (P_{max}), and the other two below and above this intensity with ratio equal to κ (NRIR). In all cases, the peak intensity of the output pulse is in good agreement with the results in Fig. 3 derived for monochromatic excitation. Furthermore, at the largest input power the response from port 2 is identical as the response from port 1 at the lowest input power, validating the fact that in Fano resonators the intensity axis of their nonlinear response is scaled by the linear asymmetry factor when we reverse the propagation direction, as was shown in Sec. II. As expected, the pulse shape is distorted due to the intensity-dependent response of the resonator, with the distortion being more severe in the high-Q case. In particular, in the high-Q case the pulse is chopped when its intensity reaches the bistability threshold of the system. This threshold is different for increasing and decreasing intensities, explaining the asymmetric shape of the output signals in Fig. 5(b). These results indicate that, although for monochromatic signals it may be possible to reach very high forward transmissivities, in practice pulse distortion may impose an upper bound on x_{lin}, and subsequently on the forward transmission.

IV. CONCLUSIONS

In this paper we have shown that passive isolators based on nonlinear resonators are subject to fundamental quantitative bounds governing the allowed levels of forward transmission versus the Q factor, input power, and nonreciprocal intensity range. In particular, we have shown that the forward transmission can increase if the Q factor or the input power increases, and the nonreciprocal intensity range correspondingly decreases. The bounds are the result of fundamental restrictions imposed by time-reversal symmetry on the field asymmetry

versus the transmission in any linear structure, and the fact that the operation of resonant nonlinear isolators is determined by their asymmetry at low intensities. We have validated our theory through full-wave simulations for the case of nonlinear isolators consisting of a dielectric metasurface on top of a substrate. Although developed for electromagnetic isolators, our analysis can be readily extended to different physical domains, such as acoustics and mechanics, in which the design of nonreciprocal devices has recently gained attention for applications in full-duplex acoustical systems, sonars, and ultrasound imaging devices [46]. Beyond clarifying several fundamental aspects of the operation of nonlinear isolators, our theory constitutes the basis for the design of such devices with optimal characteristics, operating at the bounds derived here, for the next generation of all-passive nanophotonic isolators not requiring magnetic bias. Furthermore, our analysis indicates that it may be possible to break the bounds described here in more complex systems consisting of multiple resonators supporting multistable resonant states, as we have explored herein.

APPENDIX A

Here, we will show the bound in Eq. (12). Assume that the input intensity is such that transmission in the backward direction (excitation from port 2) is zero. Then, from Eq. (4)

we find

$$x_{\mathrm{bw}} = \pm x_0,$$
$$\omega_{0,\mathrm{bw}} = \omega \pm \gamma x_0, \tag{A1}$$

where the subscript "bw" indicates that the corresponding quantity refers to the backward direction. Substituting Eq. (A1) into Eq. (8) with $i = 2$ yields

$$\left(1 + x_{\mathrm{bw}}^2\right)(x_{\mathrm{lin}} - x_{\mathrm{bw}}) = \frac{\omega_{0,\mathrm{lin}}|k_2|^2 P_{\mathrm{in}}}{\gamma^3 |a_0|^2}. \tag{A2}$$

For the same input power, Eq. (8) with $i = 1$ will give the detuning factor x_{fw} in the forward direction (excitation from port 1):

$$\left(1 + x_{\mathrm{fw}}^2\right)(x_{\mathrm{lin}} - x_{\mathrm{fw}}) = \frac{\omega_{0,\mathrm{lin}}|k_1|^2 P_{\mathrm{in}}}{\gamma^3 |a_0|^2}. \tag{A3}$$

The subscript "fw" indicates that the corresponding quantity refers to the forward direction. Transmission in the forward direction can be found by substituting x_{fw} in Eq. (4):

$$T_{\mathrm{fw}} = \frac{4\kappa}{(\kappa + 1)^2} \frac{(x_{\mathrm{fw}} - x_{\mathrm{bw}})^2}{\left(x_{\mathrm{fw}}^2 + 1\right)\left(x_{\mathrm{bw}}^2 + 1\right)}, \tag{A4}$$

where we have also used $x_0 = \pm x_{\mathrm{bw}}$ from Eq. (A1). Dividing Eqs. (A2) and (A3) yields

$$\kappa = \frac{\left(1 + x_{\mathrm{fw}}^2\right)(x_{\mathrm{lin}} - x_{\mathrm{fw}})}{\left(1 + x_{\mathrm{bw}}^2\right)(x_{\mathrm{lin}} - x_{\mathrm{bw}})}. \tag{A5}$$

Inserting Eq. (A5) into Eq. (A4) results in

$$T_{\mathrm{fw}} = \frac{4(x_{\mathrm{lin}} - x_{\mathrm{fw}})(x_{\mathrm{lin}} - x_{\mathrm{bw}})(x_{\mathrm{fw}} - x_{\mathrm{bw}})^2}{\left[\left(x_{\mathrm{fw}}^2 + 1\right)(x_{\mathrm{lin}} - x_{\mathrm{fw}}) + \left(x_{\mathrm{bw}}^2 + 1\right)(x_{\mathrm{lin}} - x_{\mathrm{bw}})\right]^2}. \tag{A6}$$

T_{fw} in Eq. (A6) is a function of two variables and through a simple analysis can be found to have a maximum value

$$T_{\mathrm{fw, max}} = \frac{1}{9 + 17x_{\mathrm{lin}}^2 - 12\sqrt{2}x_{\mathrm{lin}}\sqrt{1 + x_{\mathrm{lin}}^2}} \tag{A7}$$

for

$$x_{\mathrm{fw}} = x_{\mathrm{lin}} - \sqrt{\frac{2 - \sqrt{3}}{3}\left(1 + x_{\mathrm{lin}}^2\right)},$$
$$x_{\mathrm{bw}} = x_{\mathrm{lin}} - \sqrt{\frac{2 + \sqrt{3}}{3}\left(1 + x_{\mathrm{lin}}^2\right)}, \tag{A8}$$

or

$$x_{\mathrm{fw}} = x_{\mathrm{lin}} - \sqrt{\frac{2 + \sqrt{3}}{3}\left(1 + x_{\mathrm{lin}}^2\right)},$$
$$x_{\mathrm{bw}} = x_{\mathrm{lin}} - \sqrt{\frac{2 - \sqrt{3}}{3}\left(1 + x_{\mathrm{lin}}^2\right)}. \tag{A9}$$

Substituting Eqs. (A8) and (A9) into Eqs. (A5), we can find the values of the coordinates of the maximum points in Fig. 3. Equations (A8) lead to point A in Figs. 3(a)–3(c) and Eqs. (A9) lead to point B in Figs. 3(d)–3(f). From Eqs. (A8), (A9), and (6) we can also show that the stored energy at the condition of maximum forward transmission is given by

$$|a|_{\mathrm{max}}^2 = |a_0|^2 \frac{\gamma}{\omega_{0,\mathrm{lin}}} \sqrt{\frac{2 \pm \sqrt{3}}{3}\left(1 + x_{\mathrm{lin}}^2\right)}, \tag{A10}$$

where the plus/minus signs hold for excitation from the side of the maximum/minimum coupling coefficient.

APPENDIX B

Here, we calculate the power that is required to achieve the maximum forward transmission in Fig. 3. From Eq. (8), the input power required to achieve a certain detuning factor x_{fw} in the backward direction is given by

$$P_{\mathrm{in}} = \frac{\gamma^3 |a_0|^2}{\omega_{0,\mathrm{lin}}|k_2|^2}\left(1 + x_{\mathrm{bw}}^2\right)(x_{\mathrm{lin}} - x_{\mathrm{bw}}). \tag{B1}$$

From $2\gamma = |k_1|^2 + |k_2|^2$ and $\kappa = |k_1|^2/|k_2|^2$ it follows that $|k_2|^2 = 2\gamma/(\kappa + 1)$ and Eq. (B1) can be rewritten as

$$P_{\mathrm{in}} = \frac{\gamma^2 |a_0|^2}{2\omega_{0,\mathrm{lin}}}(\kappa + 1)\left(1 + x_{\mathrm{bw}}^2\right)(x_{\mathrm{lin}} - x_{\mathrm{bw}}). \tag{B2}$$

Substituting Eq. (A5) into Eq. (B2) yields

$$P_{\mathrm{in}} = \frac{|a_0|^2}{2} \frac{\gamma^2}{\omega_{0,\mathrm{lin}}}$$
$$\times \left[\left(1 + x_{\mathrm{fw}}^2\right)(x_{\mathrm{lin}} - x_{\mathrm{fw}}) + \left(1 + x_{\mathrm{bw}}^2\right)(x_{\mathrm{lin}} - x_{\mathrm{bw}})\right]. \tag{B3}$$

Substituting x_{fw} and x_{bw} from either Eq. (A8) or ((A9) into Eq. (B3) results in

$$P_{\mathrm{in}} = \frac{|a_0|^2}{3} \frac{\gamma^2}{\omega_{0,\mathrm{lin}}}\left(1 + x_{\mathrm{lin}}^2\right)\left(3\sqrt{2}\sqrt{1 + x_{\mathrm{lin}}^2} - 4x_{\mathrm{lin}}\right). \tag{B4}$$

This is the input power required to achieve zero transmission from port 2 and therefore infinite isolation. If x_{lin} is increased by increasing the Q factor while maintaining $\omega_{0,\mathrm{lin}} - \omega$ constant, Eq. (B4) can be written as

$$P_{\mathrm{in}} = \frac{|a_0|^2}{3} \frac{(\omega_{0,\mathrm{lin}} - \omega)^2}{\omega_{0,\mathrm{lin}}} \frac{\left(1 + x_{\mathrm{lin}}^2\right)\left(3\sqrt{2}\sqrt{1 + x_{\mathrm{lin}}^2} - 4x_{\mathrm{lin}}\right)}{x_{\mathrm{lin}}^2}, \tag{B5}$$

which, through elementary calculus, can be shown to be monotonically decreasing as x_{lin} increases within the practically important range $x_{\mathrm{lin}} \leqslant 2\sqrt{2}$. On the other hand, if the Q factor and therefore γ are constant, increasing x_{lin} results in an increase of P_{in} for $x_{\mathrm{lin}} > 0.5$.

[1] D. M. Pozar, *Microwave Engineering*, 3rd ed. (Wiley, New York, 2005).

[2] R. J. Potton, Reciprocity in optics, Rep. Prog. Phys. **67**, 717 (2004).

[3] H. B. G. Casimir, On Onsager's principle of microscopic reversibility, Rev. Mod. Phys. **17**, 343 (1945).

[4] T. Kodera, D. L. Sounas, and C. Caloz, Artificial Faraday rotation using a ring metamaterial structure without static magnetic field, Appl. Phys. Lett. **99**, 031114 (2011).

[5] T. Kodera, D. L. Sounas, and C. Caloz, Magnetless nonreciprocal metamaterial (MNM) technology: Application to microwave components, IEEE Trans. Microw. Theory Techn. **61**, 1030 (2013).

[6] Z. Wang, Z. Wang, J. Wang, B. Zhang, J. Huangfu, J. D. Joannopoulos, M. Soljačić, and L. Ran, Gyrotropic response in the absence of a bias field, Proc. Natl. Acad. Sci. USA **109**, 13194 (2012).

[7] B.-I. Popa and S. A. Cummer, Nonreciprocal active metamaterials, Phys. Rev. B **85**, 205101 (2012).

[8] Z. Yu and S. Fan, Complete optical isolation created by indirect interband photonic transitions, Nature Photon. **3**, 91 (2009).

[9] H. Lira, Z. Yu, S. Fan, and M. Lipson, Electrically Driven Nonreciprocity Induced By Interband Photonic Transition on a Silicon Chip, Phys. Rev. Lett. **109**, 033901 (2012).

[10] K. Fang, Z. Yu, and S. Fan, Photonic Aharonov-Bohm Effect Based on Dynamic Modulation, Phys. Rev. Lett. **108**, 153901 (2012).

[11] D.-W. Wang, H.-T. Zhou, M.-J. Guo, J.-X. Zhang, J. Evers, and S.-Y. Zhu, Optical Diode Made From a Moving Photonic Crystal, Phys. Rev. Lett. **110**, 093901 (2013).

[12] S. Qin, Q. Xu, and Y. E. Wang, Nonreciprocal components with distributedly modulated capacitors, IEEE Trans. Microw. Theory Techn. **62**, 2260 (2014).

[13] D. L. Sounas, C. Caloz, and A. Alù, Giant non-reciprocity at the subwavelength scale using angular momentum-biased metamaterials, Nat. Commun. **4**, 2407 (2013).

[14] R. Fleury, D. L. Sounas, C. F. Sieck, M. R. Haberman, and A. Alù, Sound isolation and giant linear nonreciprocity in a compact acoustic circulator, Science **343**, 516 (2014).

[15] D. L. Sounas and A. Alù, Angular-momentum-biased nanorings to realize magnetic-free integrated optical isolation, ACS Photon. **1**, 198 (2014).

[16] N. A. Estep, D. L. Sounas, J. Soric, and A. Alù, Magnetic-free non-reciprocity and isolation based on parametrically modulated coupled-resonator loops, Nat. Phys. **10**, 923 (2014).

[17] N. Reiskarimian and H. Krishnaswamy, Magnetic-free nonreciprocity based on staggered commutation, Nat. Commun. **7**, 11217 (2015).

[18] K. Gallo, G. Assanto, K. R. Parameswaran, and M. M. Fejer, All-optical diode in a periodically poled lithium niobate waveguide, Appl. Phys. Lett. **79**, 314 (2001).

[19] H. Zhou, K.-F. Zhou, W. Hu, Q. Guo, S. Lan, X.-S. Lin, and A. V. Gopal, All-optical diodes based on photonic crystal molecules consisting of nonlinear defect pairs, J. Appl. Phys. **99**, 123111 (2006).

[20] X.-S. Lin, W.-Q. Wu, H. Zhou, K.-F. Zhou, and S. Lan, Enhancement of unidirectional transmission through the coupling of nonlinear photonic crystal defects, Opt. Express **14**, 2429 (2006).

[21] V. Shadrivov, V. A. Fedotov, D. A. Powell, Y. S. Kivshar, and N. I. Zheludev, Electromagnetic wave analogue of an electronic diode, New J. Phys. **13**, 033025 (2011).

[22] S. Lepri and G. Casati, Asymmetric Wave Propagation in Nonlinear Systems, Phys. Rev. Lett. **106**, 164101 (2011).

[23] B. Anand, R. Podila, K. Lingam, S. R. Krishnan, S. S. S. Sai, R. Philip, and A. M. Rao, Optical diode action from axially asymmetric nonlinearity in an all-carbon solid-state device, Nano Lett. **13**, 5771 (2013).

[24] B. Peng, S. K. Özdemir, F. Lei, F. Monifi, M. Gianfreda, G. L. Long, S. Fan, F. Nori, C. M. Bender, and L. Yang, Parity–time-symmetric whispering-gallery microcavities, Nat. Phys. **10**, 394 (2014).

[25] X.-S. Lin, J.-H. Yan, L.-J. Wu, and S. Lan, High transmission contrast for single resonator based all-optical diodes with pump-assisting, Opt. Express **16**, 20949 (2008).

[26] S. Manipatruni, J. T. Robinson, and M. Lipson, Optical Nonreciprocity in Optomechanical Structures, Phys. Rev. Lett. **102**, 213903 (2009).

[27] E. Miroshnichenko, E. Brasselet, and Y. S. Kivshar, Reversible optical nonreciprocity in periodic structures with liquid crystals, Appl. Phys. Lett. **96**, 063302 (2010).

[28] D. Roy, Few-photon optical diode, Phys. Rev. B **81**, 155117 (2010).

[29] S. V. Zhukovsky and A. G. Smirnov, All-optical diode action in asymmetric nonlinear photonic multilayers with perfect transmission resonances, Phys. Rev. A **83**, 023818 (2011).

[30] P. Aleahmad, M. Khajavikhan, D. Christodoulides, and P. LiKamWa, Integrated multi-port circulators for unidirectional optical information transport, Sci. Rep. **7**, 2129 (2017).

[31] L. Fan, J. Wang, L. T. Varghese, H. Shen, B. Niu, Y. Xuan, A. M. Weiner, and M. Qi, An all-silicon passive optical diode, Science **335**, 447 (2012).

[32] L. Fan, L. T. Varghese, J. Wang, Y. Xuan, A. M. Weiner, and M. Qi, Silicon optical diode with 40 dB nonreciprocal transmission, Opt. Lett. **38**, 1259 (2013).

[33] Y. Xu, and A. E. Miroshnichenko, Reconfigurable nonreciprocity with a nonlinear Fano diode, Phys. Rev. B **89**, 134306 (2014).

[34] Y. Yu, Y. Chen, H. Hu, W. Xue, K. Yvind, and J. Mork, Nonreciprocal transmission in a nonlinear photonic-crystal Fano structure with broken symmetry, Laser Photon. Rev. **9**, 241 (2015).

[35] M. Mahmoud, A. R. Davoyan, and N. Engheta, All-passive nonreciprocal metastructure, Nat. Commun. **6**, 8359 (2015).

[36] W. Ding, B. Luk'yanchuk, and C.-W. Qiu, Ultrahigh-contrast-ratio silicon Fano diode, Phys. Rev. A **85**, 025806 (2012).

[37] Y. Shi, Z. Yu, and S. Fan, Limitations of nonlinear optical isolators due to dynamic reciprocity, Nature Photon. **9**, 388 (2015).

[38] S. Trendafilov, V. Khudik, M. Tokman, and G. Shvets, Hamiltonian description of non-reciprocal light propagation in nonlinear chiral fibers, Physica B **405**, 3003 (2010).

[39] R. W. Boyd, *Nonlinear Optics*, 3rd ed. (Academic, New York, 2008).

[40] S. Fan and J. D. Joannopoulos, Analysis of guided resonances in photonic crystal slabs, Phys. Rev. B **65**, 235112 (2002).

[41] H. A. Haus, *Waves and Fields in Optoelectronics* (Prentice-Hall, Englewood Cliffs, NJ, 1984).

[42] D. L. Sounas and A. Alù, Time-reversal Symmetry Bounds on the Electromagnetic Response of Asymmetric Structures, Phys. Rev. Lett. **118**, 154302 (2017).

[43] K. X. Wang, Z. Yu, S. Sandhu, and S. Fan, Fundamental bounds on decay rates in asymmetric single-mode optical resonators, Opt. Lett. **38**, 100 (2013).

[44] A. Rodriguez, M. Soljacic, J. D. Joannopoulos, and S. G. Johnson, Chi(2) and chi(3) harmonic generation at a critical power in inhomogeneous doubly resonant cavities, Opt. Express **15**, 7303 (2007).

[45] D. L. Sounas, J. Soric, and A. Alù, Broadband passive isolators based on coupled nonlinear resonances, Nat. Electron. **1**, 113 (2018).

[46] R. Fleury, D. L. Sounas, M. Haberman, and A. Alù, Non-reciprocal acoustics, Acoustics Today **11**, 14 (2015).